

Computer simulation of plane electromagnetic wave
propagation in a waveguide formed by the Earth's surface
and ionosphere under the condition of inhomogeneous
conductivity of the boundaries

XIII International Conference Solar-Terrestrial Relations And Physics Of
Earthquakes Precursors

Tverdyi D.A., Malkin E.I., Parovik R.I.

Institute of Cosmophysical Research and Radio Wave Propagation FEB RAS, Russia, Kamchatka
State, Paratunka, Mirnaya St., 7;

25–29 September, 2023
Paratunka, Russia

Atmospherics

According to WWLLN (The World Wide Lightning Location Network), up to 50 lightning strikes occur on earth every second. Lightning discharges in thunderstorm clouds generate naturally occurring electromagnetic radiation.

This allows us to consider lightning discharges as constantly acting sources of pulsed electromagnetic radiation (atmospherics) [Koronczay, 2019] [Lichtenberger J., 2008, Storey L. 1953].

Definition 1

Atmospheric is a broadband signal with maximum intensity in the 6-10 kHz range.

However, atmospheric propagates not in free space, but in the complex conductive structure of a waveguide [Budden and Eve, 1975].

Earth-ionosphere waveguide

A waveguide is a structure that directs waves, such as electromagnetic waves or sound, with minimal energy loss by limiting energy transfer in one direction [Sarkar et al., 2006].

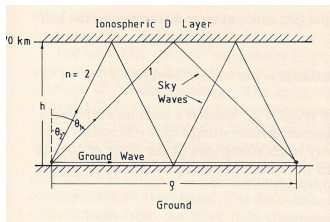


Figure 1: Geometry of ray propagation in the surface ionospheric waveguide (Earth-ionosphere waveguide)

Ionospheric waveguide – the region of space between the Earth's surface and the ionosphere (or between layers of the ionosphere [Wait, 1970]). An example is shown in (Fig. 1), which illustrates localized radio wave propagation [Spies and Wait, 1961].

Definition 2

In a surface ionospheric waveguide (Earth-ionosphere waveguide), the lower boundary is the Earth's surface and the upper boundary is one of the ionospheric layers (Fig. 1).

Inhomogeneities at the waveguide boundary

Atmospheric propagation [Helliwell, 2006, Helliwell and Pytte, 1966] has an imminent interaction with inhomogeneities in the waveguide.

These inhomogeneities are caused by changes in the conductivity of the waveguide walls in the direction of atmospheric propagation. They can exist permanently (coastal line of oceans), or be temporarily occurring (local conductivity change).

In turn, the local change in conductivity can be caused by changes in the chemical composition of subsurface near-surface water [Копылова et al., 2018].

Water is known to be a good conductor. However, secondary minerals may appear in the composition of water due to geological activity.

There may also be non-electrically conductive CO_2 as part of the free gases dissolved in the water. Deep CO_2 emissions characterize many seismically active regions around the world [Chiodini et al., 2020].

Such impurities in the composition of subsurface near-surface water may be the cause of conductivity inhomogeneities.

Presumably, this could link the changes in earth conductivity (inhomogeneity) modeled in this study and some hydrogeochemical precursors to earthquakes weeks to months before they occur.

System of Maxwell's equations

In many problems of modeling electromagnetic phenomena (and in particular computational electromagnetics), the starting point will be Maxwell's fundamental equations [Maxwell, 1865]. Formulated more than a century and a half ago, they are still in great demand:

$$\nabla \times \vec{H} = \frac{\partial \vec{D}}{\partial t} + \vec{J}, \quad (1a)$$

$$\nabla \times \vec{E} = -\frac{\partial \vec{B}}{\partial t} - \vec{M}, \quad (1b)$$

$$\nabla \cdot \vec{D} = \rho_e, \quad (1c)$$

$$\nabla \cdot \vec{B} = \rho_m. \quad (1d)$$

Given the additional relations [Nickelson, 2018, page 202] defining the free space, the equations (1) can be rewritten as:

$$\nabla \times \vec{H} = \varepsilon \frac{\partial \vec{E}}{\partial t} + \sigma^e \vec{E} + \vec{J}_i, \quad (2a)$$

$$\nabla \times \vec{E} = -\mu \frac{\partial \vec{H}}{\partial t} - \sigma^m \vec{H} - \vec{M}_i, \quad (2b)$$

где

- σ^e — conductivity [siemens/meter];
- σ^m — magnetic conductivity [ohms/meter].

Remark 1

Using σ^e and σ^m , known for each point in the mathematical model, we will specify the inhomogeneities of the waveguide walls.

Next, we present the vector equations (2) in scalar form of 6 equations for the Cartesian coordinate system (x, y, z) , which can be viewed as two separate systems of equations (modes) of 3 equations.

In our case, we will consider the problem in a 2-dimensional section. I.e. when the geometry of the problem and the distribution of fields in one dimension does not change, let this be the y axis. Then the motion of the (electric) component \vec{E} and the (magnetic) component \vec{H} along the x and z axes are of interest. To do this, in Maxwell's equations (2) we put the derivative: $\partial y = 0$.

Remark 2

In our research, only the TE_y (Transverse Electric y) mode is of interest:

$$\frac{\partial E_x}{\partial t} = \frac{1}{\epsilon_x} \left[-\frac{\partial H_y}{\partial z} - \sigma_x^e E_x - J_{ix} \right], \quad (3a)$$

$$\frac{\partial E_z}{\partial t} = \frac{1}{\epsilon_z} \left[\frac{\partial H_y}{\partial x} - \sigma_z^e E_z - J_{iz} \right], \quad (3b)$$

$$\frac{\partial H_y}{\partial t} = \frac{1}{\mu_y} \left[\frac{\partial E_z}{\partial x} - \frac{\partial E_x}{\partial z} - \sigma_y^m H_y - M_{iy} \right], \quad (3c)$$

The FDTD method for numerical solution

The Finite-Difference Time-Domain (FDTD) method or Yee's Algorithm [Yee, 1966], was one of the first methods to numerically solve (1) on spatial grid and has remained the subject of continuous development.

The fact that Maxwell's equations (1) are actually hyperbolic PDE is the basis of the entire FDTD method. That is, for (1) there are solutions that behave like waves, and the disturbance propagates at a finite speed.

Remark 3

Moreover, when deriving the numerical scheme of the FDTD method, we need to consider only equations (1a) and (1b), and the divergence equations (1c) and (1d) will be satisfied by the developed equations of the numerical scheme [Taflove and Hagness, 2005, page. 60]. Since they are implicitly included in the update equations of the spatial components (x, y, z) of the \vec{E} and \vec{H} fields of the FDTD, which can be clearly seen in Figure 2.

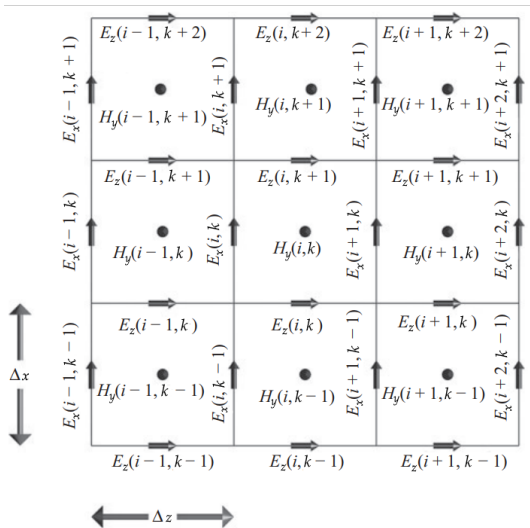


Figure 2: The position of the (x, y, z) components of the vectors \vec{E} and \vec{H} relative to the unit 2-D cell in the FDTD grid, for the calculation of the TE_y mode [Chen, 2005, page 635, Figure 9.1]

Boundary conditions problem

The need for boundary conditions arises at least because the cell structure of the Yi algorithm inevitably leads to a problem with computing points at the edge of the grid.

For example, for TE_y , we can see from Figure 2 that the computation of the E_z and E_x components depends on the values of H_y on either side of E_z and E_x , respectively. However, there are no such E_z and E_x – components in the outermost cells that have both H_y .

Remark 4

This is a problem that is obviously not solved by adding an extra row of cells to the problem position.

Perfectly matched layer (PML)

The simplest approach is to set the boundary values of the calculated components equal to 0. But then they act as Perfect electric conductor (PEC), and thus completely reflect the incident waves.

However, there are conditions called Absorbing boundary conditions (ABC) that simulate a transparent (zero reflection coefficient) boundary regardless of the frequency, polarization and angle of incidence of the signal.

Research in this area has led to PML [Berenger, 1994], i.e., an absorbing medium bordering the outer planes of the spatial lattice of the modeled region.

Remark 5

PML is an excellent solution for truncating FDTD gratings, when modeling signal propagation in different lossy materials or waveguides. Since extremely small numerical wave reflection coefficients on the order of 10^{-6} and 10^{-8} can be achieved with acceptable computational load.

Definition 3

PML is given by certain conductivities σ^e and σ^m , so that outgoing waves penetrate without reflection and attenuate while traveling in the PML medium. And the papers [Andrew et al., 1995] [Berenger, 1996] [Veihl and Mittra, 1996] [Gedney, 1996] show the high stability of PML as ABC.

Remark 6

An important feature is that σ^e and σ^m (hereinafter referred to as conductivity profiles) in the PML region should increase smoothly. Otherwise, due to a sharp jump in the values of conductivity profiles, PEC-like reflections occur.

Given that at the edge of the entire PEC region, we can now numerically model the conduction inhomogeneities of the waveguide wall.

Setting boundary inhomogeneities with σ^e and σ^m

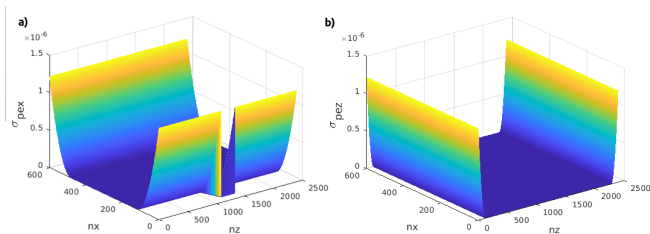


Figure 3: Example of setting the inhomogeneity of the earth-ionosphere waveguide boundary in simulation. Conductivity profile σ^e for the inhomogeneity in the 1nd approximation

We set the inhomogeneity of the waveguide boundary by changing the values of σ^e and σ^m for PML in some region, as in Figure 3. Then the part of the signal that moves at an angle to the waveguide boundary will not be absorbed by the PML and the region of interest, will be reflected from the PEC, and will cause the observed back wave in the region modeling the waveguide. This should be confirmed by numerical experiment.

FDTD discretization with PML consideration

Usually, how the signal will propagate in the PML region is calculated by separate equations for the appropriate regions.

This is done because the signal motion in the PML (wall) region is described by the equations for free space, while the inner region could potentially model any other material or medium defined by a somewhat different equation.

Definition 4

However, in our problem the inner region is also a free space as well as the walls. Therefore, the final version of the formulas of the FDTD numerical scheme can be written for the whole region at once.

Also there is a need to decompose H_y in the equation (3c) two artificial components $H_y = H_{yz} + H_{yx}$ along the directions z and x , in the PML region.

For more detailed information on FDTD schemes in other cases, see [Elsherbeni and Demir, 2015, page. 13–29], as well as in the book [Taflove and Hagness, 2005, page 62–74].

$$\varepsilon_0 \frac{\partial E_z}{\partial t} + \sigma_{pex} E_z = \frac{\partial (H_{yz} + H_{yx})}{\partial x}, \quad (4a)$$

$$\varepsilon_0 \frac{\partial E_x}{\partial t} + \sigma_{pez} E_x = -\frac{\partial (H_{yz} + H_{yx})}{\partial z}, \quad (4b)$$

$$\mu_0 \frac{\partial H_{yz}}{\partial t} + \sigma_{pmz} H_{yz} = -\frac{\partial E_x}{\partial z}, \quad (4c)$$

$$\mu_0 \frac{\partial H_{yx}}{\partial t} + \sigma_{pmx} H_{yx} = \frac{\partial E_z}{\partial x}. \quad (4d)$$

where σ_{pez} – this is σ^e along Oz , σ_{pex} – this is σ^e along Ox , fictitious conductivity. For σ^m it's all the same.

Next, we present a discrete version of the formulas, where: Δx , Δz – increments of the lattice space in the coordinate directions x , z , respectively; indices i , k are integers denoting the cell number in the space; Δt – time increment, which is assumed to be uniform over the observation interval; n is an integer.

Component $E_z^{n+1}(i, k)$:

$$E_z^{n+1}(i, k) = C_{eze}(i, k) \times E_z^n(i, k) + C_{ezhy}(i, k) \times \left(H_{yz}^{n+1/2}(i, k) - H_{yz}^{n+1/2}(i, k-1) + H_{yx}^{n+1/2}(i, k) - H_{yx}^{n+1/2}(i, k-1) \right), \quad (5a)$$

where,

$$C_{eze}(i, k) = \frac{2\varepsilon_z - \Delta t \sigma_{pex}(i, k)}{2\varepsilon_z + \Delta t \sigma_{pex}(i, k)}, \quad (5b)$$
$$C_{ezhy}(i, k) = \frac{2\Delta t}{(2\varepsilon_z + \Delta t \sigma_{pex}(i, k)) \Delta x}.$$

Component $E_x^{n+1}(i, k)$:

$$E_x^{n+1}(i, k) = C_{exe}(i, k) \times E_x^n(i, k) + C_{exhy}(i, k) \times \left(H_{yz}^{n+1/2}(i, k) - H_{yz}^{n+1/2}(i-1, k) + H_{yx}^{n+1/2}(i, k) - H_{yx}^{n+1/2}(i-1, k) \right), \quad (6a)$$

where,

$$C_{exe}(i, k) = \frac{2\varepsilon_x - \Delta t \sigma_{pez}(i, k)}{2\varepsilon_x + \Delta t \sigma_{pez}(i, k)}, \quad (6b)$$
$$C_{exhy}(i, k) = -\frac{2\Delta t}{(2\varepsilon_x + \Delta t \sigma_{pez}(i, k)) \Delta z}.$$

Component $H_{yz}^{n+1/2}(i, k)$:

$$H_{yz}^{n+1/2}(i, k) = C_{hyzh}(i, k) \times H_{yz}^{n-1/2}(i, k) + C_{hyzex}(i, k) \times (E_x^n(i+1, k) - E_x^n(i, k)), \quad (7a)$$

where,

$$C_{hyzh}(i, k) = \frac{2\mu_y - \Delta t \sigma_{pmz}(i, k)}{2\mu_y + \Delta t \sigma_{pmz}(i, k)}, \quad (7b)$$
$$C_{hyzex}(i, k) = -\frac{2\Delta t}{(2\mu_y + \Delta t \sigma_{pmz}(i, k)) \Delta z}.$$

Component $H_{yx}^{n+1/2}(i, k)$:

$$H_{yx}^{n+1/2}(i, k) = C_{hyxh}(i, k) \times H_{yx}^{n-1/2}(i, k) + C_{hyxex}(i, k) \times (E_z^n(i, k+1) - E_z^n(i, k)), \quad (8a)$$

where,

$$C_{hyxh}(i, k) = \frac{2\mu_y - \Delta t \sigma_{pmx}(i, k)}{2\mu_y + \Delta t \sigma_{pmx}(i, k)}, \quad (8b)$$
$$C_{hyxex}(i, k) = \frac{2\Delta t}{(2\mu_y + \Delta t \sigma_{pmx}(i, k)) \Delta x}.$$

Computational experiment 1

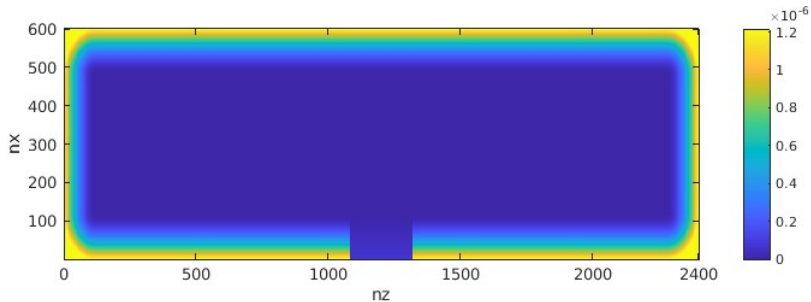


Figure 4: Conductivity profile σ^e for the inhomogeneity in the 1st approximation

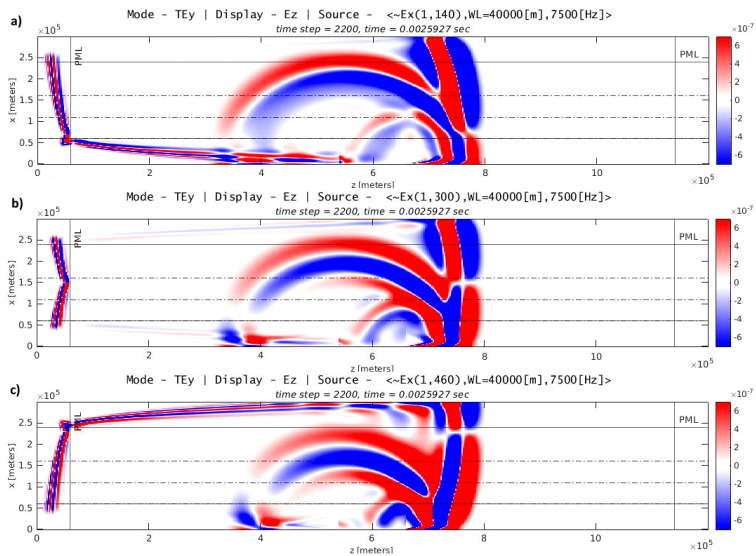


Figure 5: Experiments: a) source $S_3(t)$; b) source $S_2(t)$; c) source $S_1(t)$

Computational experiment 2

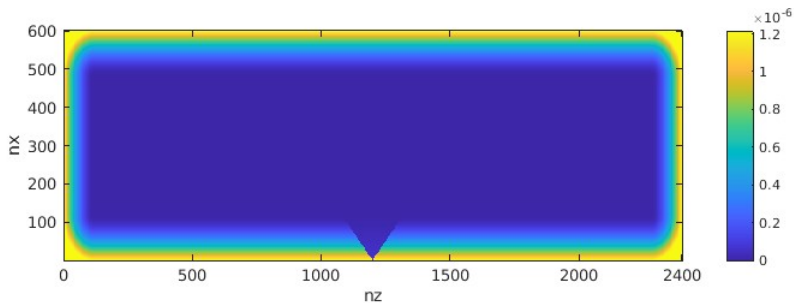


Figure 6: Conductivity profile σ^e for the inhomogeneity in the 2nd approximation

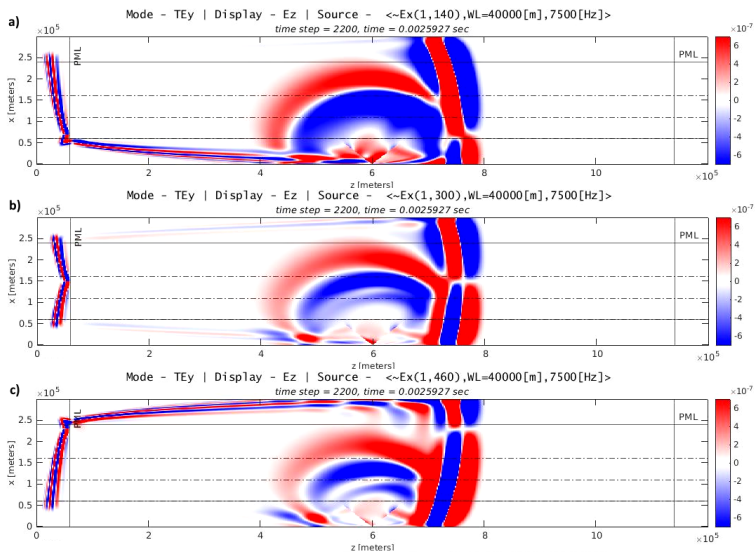


Figure 7: Experiments: a) source $S_3(t)$; b) source $S_2(t)$; c) source $S_1(t)$

Computational experiment 3

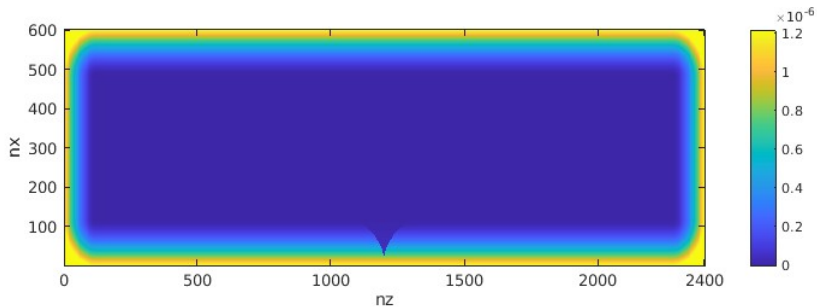


Figure 8: Conductivity profile σ^e for the inhomogeneity in the 3rd approximation

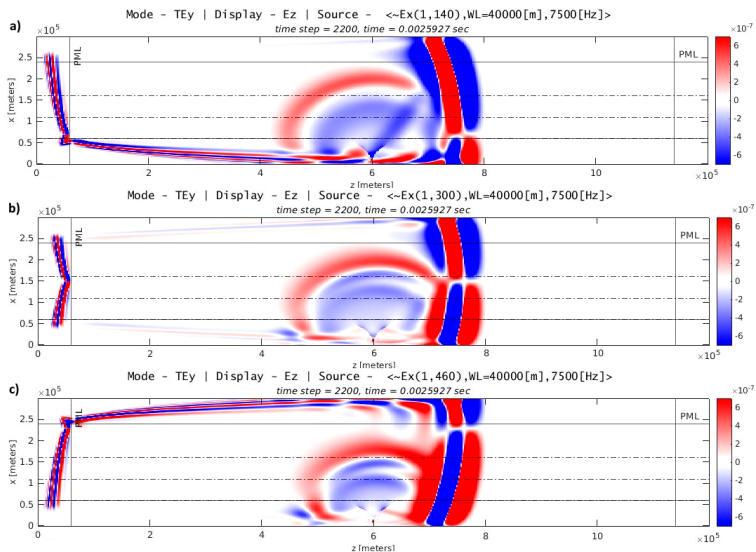


Figure 9: Experiments: a) source $S_3(t)$; b) source $S_2(t)$; c) source $S_1(t)$

Conclusion

By using mathematical modeling and computer simulations of the process of interaction of EM waves with inhomogeneity of the lower boundary (ground) of the waveguide, it is shown that:

1. indeed, there is backscattering of the EM wave on the waveguide trace;
2. backscattering occurs due to reflection of EM wave, when it interacts with inhomogeneity of conductivity of the lower boundary of the waveguide;
3. for different approximations of conductivity inhomogeneities, backscattering waves with different intensities and different arrival times are observed;

Indeed, mathematical and computer modeling of the process can help in establishing the relationship between radiation parameters and inhomogeneities.

One can assume that the reverse is also true: observation of EM signal parameters defining the atmospheric, including the sometimes observed backscattering wave, allows us to establish the presence of conductivity inhomogeneity on the propagation trace.

Discussion

The next stage of research will be to isolate the effects of inhomogeneities of the upper boundary of the waveguide (ionosphere) from EM data of atmospheric observations, using satellite tomography data.

Eliminating their effects on the parameters of the atmospheric EM wave, the remaining effects caused by inhomogeneities of conductivity can be explained by the fact that they are caused precisely by inhomogeneities along the lower (ground) boundary.

Further, based on the parameters of the backscattering wave from the atmospheric EM wave, it will be possible to determine the direction of arrival of the backscattering wave, and therefore the location of the assumed inhomogeneity.

Proceeding from the fact that, such a local change in conductivity can be caused by a change in the chemical composition of underground subsoil waters as a consequence of geologic activity predecessor to earthquakes. It will be possible to test the hypothesis that there is a relationship between the parameters of the atmospheric and some hydrogeochemical precursors of earthquakes.

Работа выполнена в рамках Государственного задания по теме (2021—2023 гг.) "Физические процессы в системе ближнего космоса и геосфер при солнечных и литосферных воздействиях", регистрационный номер AAAA-A21-121011290003-0

The work was carried out within the framework of the State task on the topic (2021—2023) "Physical processes in the system of near space and geospheres under solar and lithospheric impact", registration number AAAA-A21-121011290003-0

Thank you for your attention!



Andrew, W. V., Balanis, C. A., and Tirkas, P. A. (1995).
Comparison of the berenger perfectly matched layer and the lindman
higher-order abc's for the fdtd method.
IEEE Microwave and Guided Wave Letters, 5(6):192–194.



Berenger, J. P. (1994).
A perfectly matched layer for the absorption of electromagnetic waves.
Journal of Computational Physics, 114(2):185–200.



Berenger, J. P. (1996).
Perfectly matched layer for the fdtd solution of wave-structure interaction
problems.
IEEE Transactions on Antennas and Propagation, 44(1):110–117.



Budden, K. G. and Eve, M. (1975).
Degenerate modes in the earth-ionosphere waveguide.
*Proceedings of The Royal Society A: Mathematical, Physical and Engineering
Sciences*, 342(1629):175–190.

Список литературы II



Chen, W. K. (2005).
The Electrical Engineering Handbook.
Elsevier, Amsterdam.



Chiodini, G., Cardellini, C., Luccio, F. D., Selva, J., Frondini, F., Caliro, S., Rosiello, A., Beddini, G., and Ventura, G. (2020).
Correlation between tectonic CO_2 earth degassing and seismicity is revealed by a 10-year record in the apennines, italy.
Science Advances, 6(35):eabc2938.



Elsherbeni, A. Z. and Demir, V. (2015).
The finite-difference time-domain method for electromagnetics with MATLAB simulations, volume 2.
SciTech Publishing, Raleigh, USA.



Gedney, S. D. (1996).
An anisotropic perfectly matched layer-absorbing medium for the truncation of fdtd lattices.
IEEE transactions on Antennas and Propagation, 44(12):1630–1639.

Список литературы III

-  Helliwell, R. A. (2006).
Whistlers and Related Ionospheric Phenomena.
Dover Publications, New York, USA.
-  Helliwell, R. A. and Pytte, A. (1966).
Whistlers and related ionospheric phenomena.
American Journal of Physics, 34(1):81–81.
-  Koronczay, D., L. J. C. M. A. R. C. J. L. S. S. D. V. e. a. (2019).
The source regions of whistlers.
Journal of Geophysical Research: Space Physics, 124:5082–5096.
-  Lichtenberger J., Ferencz C., B. L. H. D. S. P. (2008).
Automatic whistler detector and analyzer system: Automatic whistler detector.
J. Geophys. Res., 113(A12):5082–5096.

Список литературы IV



Maxwell, J. C. (1865).

Viii. a dynamical theory of the electromagnetic field.

Philosophical Transactions of the Royal Society of London, 155:459–512.



Nickelson, L. (2018).

Electromagnetic Theory and Plasmonics for Engineers.

Singapore: Springer.



Sarkar, T. K., Mailloux, R. J., Oliner, A. A., Palma, M. S., and Sengupta, D. L. (2006).

The Evolution of Electromagnetic Waveguides: From Hollow Metallic Guides to Microwave Integrated Circuits, pages 543–566.

John Wiley & Sons, New-York, USA.



Spies, K. P. and Wait, J. R. (1961).

Mode calculations for VLF propagation in the earth-ionosphere waveguide.

U.S. Dept. of Commerce, Washington, USA.

-  Storey L. R. O. (1953).
An investigation of whistling atmospherics.
Philosophical Transactions of the Royal Society of London. Series A, Mathematical and Physical Sciences, 246(908):113–141.
-  Taflove, A. and Hagnes, S. C. (2005).
Computational Electrodynamics: The Finite-difference Time-domain Method.
Artech House, Massachusetts, USA.
-  Veihl, J. C. and Mittra, R. (1996).
Efficient implementation of berenger's perfectly matched layer (pml) for
finite-difference time-domain mesh truncation.
IEEE Transactions on Antennas and Propagation, 6(2):94–96.
-  Wait, J. R. (1970).
Electromagnetic Waves in Stratified Media.
Oxford University Press, Oxford, UK.



Yee, K. (1966).

Numerical solution of initial boundary value problems involving maxwell's equations in isotropic media.

IEEE Transactions on Antennas and Propagation, 14(3):302–307.



Копылова, Г. Н., Гусева, Н. В., Копылова, Ю. Г., and Болдина, С. В. (2018).

Химический состав подземных вод режимных водопроявлений Петропавловского геодинамического полигона, Камчатка: типизация и эффекты сильных землетрясений.

Journal of Volcanology and Seismology, (4):43–62.